****

SOME STUDIES OF AN ERROR ESTIMATOR BASED ON A PATCH RECOVERY SCHEME
PART I - THE PATCH RECOVERY SCHEME

by A.C.A. Ramsay* & H. Sbresny**

****

SUMMARY

In this article, the recently proposed patch recovery scheme of Zienkiewicz and Zhu [4] is applied to the basic four-node isoparametric displacement membrane. The common configuration of a four element patch is considered. It is observed, for this element and configuration, that the proposed scheme can produce results that are dependent on the co-ordinate system in which the patch is defined. In attempting to overcome this problem the concept of a parent patch is proposed. Results from an error estimator based on this concept and applied to a set of problems similar to those laid down in [3] are presented.

INTRODUCTION

Whereas, in general, the true stress field $\{\sigma\}$ is continuous, the finite element stress field $\{\sigma_h\}$ is generally discontinuous across element interfaces as illustrated for a single component of stress on a patch of four elements in Figure 1(a). This lack of continuity has traditionally been used for qualitative assessment of a finite element model, and more recently as a means to quantify the error in a model.

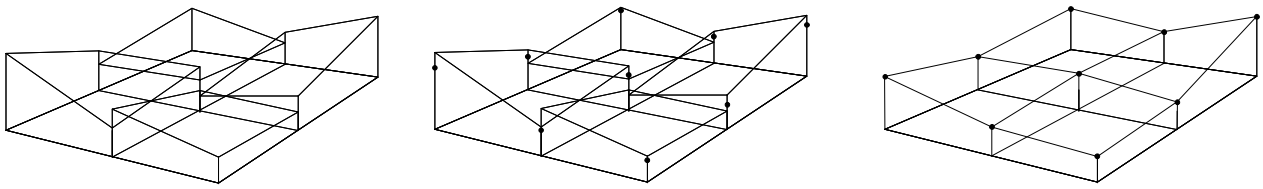

(a) Discontinuous σ_h (b) Unique nodal stresses (c) Continuous $\tilde{\sigma}$

Figure 1 Achieving continuous estimated stress fields from discontinuous finite element stress fields

Although the true error $\{\sigma_e\}=\{\sigma\}-\{\sigma_h\}$ is usually unknown, an estimated error $\{\tilde{\sigma}_e\}=\{\tilde{\sigma}\}-\{\sigma_h\}$ can be formed by assuming an estimated stress field $\{\tilde{\sigma}\}$. Of the many ways in which an estimated stress field may be formed, those that determine $\{\tilde{\sigma}\}$ such that it is continuous across element interfaces have received much attention [1],[2]. Continuous estimated stress fields are defined by interpolating unique nodal stresses $\{s\}$ over an element with the matrix $\left[\overline{N}\right]$ which contains the same polynomial terms as the element shape functions. Thus, for an element, $\{\tilde{\sigma}\}$ is defined as:

$$\underset{(3x12)}{\{\tilde{\sigma}\}=\left[\overline{N}\right]\{s\}} \tag{1}$$

* Postgraduate, Robinson FEM Inst., Univ. of Exeter, England.
** ERASMUS Student, Dept. of Aero. Eng., Univ. of Stuttgart, Germany.

Given an estimated stress field $\{\tilde{\sigma}\}$, error measures such as the estimated percentage error $\tilde{\alpha}$ can then be formed for the element and for the model. The reader is referred to Part I of the FEN articles [3] for a full description of the error measures used in this article.

For the estimated stress field defined in Equation (1), different choices for the unique nodal stresses $\{s\}$ will result in different estimated stress fields $\{\tilde{\sigma}\}$ and, therefore, different error measures $\tilde{\alpha}$. A number of so-called simple error estimators in which the unique nodal stresses are chosen simply as the averaged nodal stresses were studied in Parts II - VI of the FEN articles [3].

An alternative method in which the unique nodal stresses are determined through a *patch recovery scheme* has been proposed in [4] and is illustrated for the considered configuration in Figure 2. In the patch recovery scheme, for each component of stress, a polynomial stress surface σ_p (shown hatched in Figure 2), with the same polynomial terms as the element shape functions, is fitted in a least squares manner to the finite element stresses at the superconvergent (stress) points [6] in the elements of the patch. For the element under consideration there is a single superconvergent point at the isoparametric centre of the element.

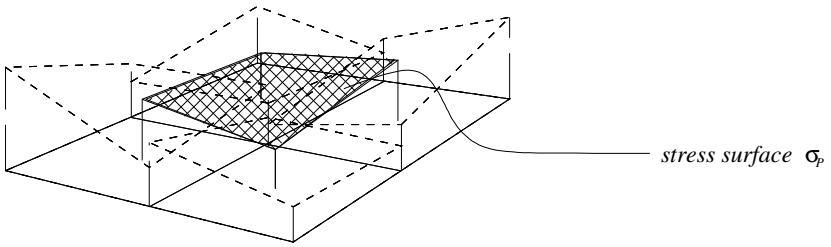

Figure 2 Patch recovery scheme for a patch of four elements

The stress surface is defined as

$$\underset{(1x4)}{\sigma_p} = \underset{(1x4)}{\lfloor P \rfloor} \underset{(4x1)}{\{a\}} \tag{2}$$

where $\sigma_p = \sigma_{px}$, σ_{py} or τ_{pxy} and, for the element under consideration in which the shape functions are bi-linear, the row vector $\lfloor P \rfloor = \lfloor 1, x, y, xy \rfloor$.

The component of unique nodal stress (*recovered stress*) is determined by evaluating Equation (2) at the appropriate node (*patch recovery point).* The vector $\{a\}$, which is different for each component of stress, is determined by solving the matrix equation resulting from the least squares fit:

$$\underset{(4x4)}{[A]} \underset{(4x1)}{\{a\}} = \underset{(4x1)}{\{b\}} \tag{3}$$

where $[A] = \sum_{i=1}^{n} \lfloor P \rfloor_i^T \lfloor P \rfloor_i$, $\{b\} = \sum_{i=1}^{n} \lfloor P \rfloor_i^T \sigma_{hi}$, the summation is taken over all n elements in the patch and $\sigma_{hi} = \sigma_{hx}$, σ_{hy} or τ_{hxy} evaluated at superconvergent point i. For the configuration considered in this article $n = 4$.

DEPENDENCE ON CO-ORDINATE SYSTEM

In their *original* paper [4], Zienkiewicz and Zhu make no mention of the co-ordinate system chosen for the patch recovery scheme. In the absence of any evidence to the contrary, one might be tempted

to think that the patch recovery scheme yields results that are independent of the chosen co-ordinate system. Unfortunately, though, this is not the case. The dependence on the co-ordinate system manifests itself in three ways:

(i) dependence on the position of the patch (l -dependence)
(ii) dependence on the size of the patch (r -dependence)
(iii) dependence on the orientation of the patch (θ-dependence)

The first two dependencies can be avoided by using the normalized local patch co-ordinate system subsequently communicated by Zienkiewicz, Zhu and Wu [5]. However, this co-ordinate system does not remove the dependency on the orientation of the patch. In this article a parent patch concept is used to define a patch co-ordinate system which yields results that, in addition to being independent of position and size, are also independent of the orientation of the patch. The various aspects of dependence are now described.

a) Dependence on position of the patch (l -dependence)

Consider a patch of four rectangular elements as shown in Figure 3. For this configuration the patch recovery point is coincident with the centre of the superconvergent points. The patch is displaced from the origin of a co-ordinate system (x, y) by a length l .

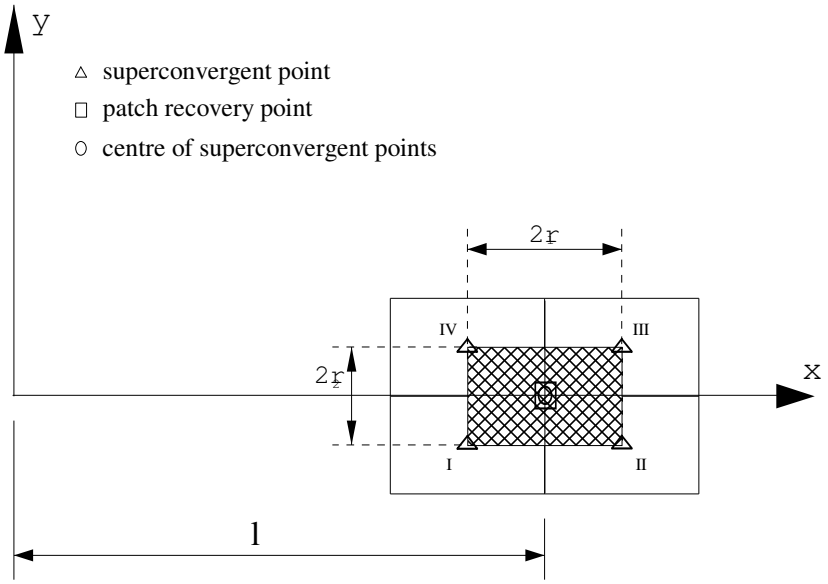

Figure 3 Element patch to show dependence on position and size of patch

The influence of the length l on the matrix $[A]$ (l -dependence) can be clearly seen by considering the case when $r_1 = r_2 = r$. If we define the parameter $\phi = l/r$ then the matrix $[A]$ may be written as

$$[\mathrm{A}] = \begin{bmatrix} 4 & 4r\phi & 0 & 0 \\ 4r\phi & 4r^2(\phi^2+1) & 0 & 0 \\ 0 & 0 & 4r^2 & 4\phi r^3 \\ 0 & 0 & 4\phi r^3 & 4r^4(\phi^2+1) \end{bmatrix} \tag{4}$$

For $l >> r$ ($\phi >> 1$), the matrix $[A]$ tends to

$$[\mathrm{A}] = \begin{bmatrix} 4 & 4r\phi & 0 & 0 \\ 4r\phi & 4r^2\phi^2 & 0 & 0 \\ 0 & 0 & 4r^2 & 4\phi r^3 \\ 0 & 0 & 4\phi r^3 & 4r^4\phi^2 \end{bmatrix} \tag{5}$$

where it is observed that the components of the matrix $[A]$

$$A_{2,i} = r\phi A_{1,i} = lA_{1,i} \text{ and } A_{4,i} = r\phi A_{3,i} = lA_{3,i} \text{ and } i = 1,2,3 \text{ or } 4 \tag{6}$$

There is a linear dependence between rows 1&2 and rows 3&4 and, therefore, the matrix $[A]$ is singular and rank deficient by two. Thus, when ϕ is large the matrix $[A]$ will be ill-conditioned and the recovered stress values will be sensitive to computational round-off in the solution of Equation (3).

b) Dependence on size of patch (r -dependence)

In order to examine the influence of the size of the element patch on the matrix $[A]$ (r -dependence) we shall consider the case where $l \to 0$ ($\phi \to 0$). In this case the matrix $[A]$ tends to

$$[\mathrm{A}] = \begin{bmatrix} 4 & 0 & 0 & 0 \\ 0 & 4r^2 & 0 & 0 \\ 0 & 0 & 4r^2 & 0 \\ 0 & 0 & 0 & 4r^4 \end{bmatrix} \tag{7}$$

This matrix has perfect condition when $r = 1$ unit of length. However, for r significantly greater than unity $A_{4,4} >> A_{1,1}$ and for r significantly less than unity $A_{4,4} << A_{1,1}$. Thus for r significantly different from unity the matrix $[A]$ becomes ill-conditioned. This situation may have a practical significance in refined meshes where r becomes small. Indeed, depending on the system of length units in which r is specified, $[A]$ may be either well- or ill-conditioned (consider $r = 1m = 1000mm$).

It is seen then that, for a fixed r, the condition of the matrix $[A]$ is strongly dependent on the position of the element patch in the co-ordinate system and deteriorates the further the centre is from the origin. One way to overcome this dependency is to use a co-ordinate system that is local to the patch. In order to avoid the problem of ill-conditioning due to the size of the patch, one could choose to use a co-ordinate system that is normalized with respect to the dimensions of the patch. The use of such a normalized local patch co-ordinate system $(\bar{x}, \bar{y})$, in which $-1 \le \bar{x} \le 1$ and $-1 \le \bar{y} \le 1$, has been recommended in a subsequent communication [5] and is shown in Figure 4.

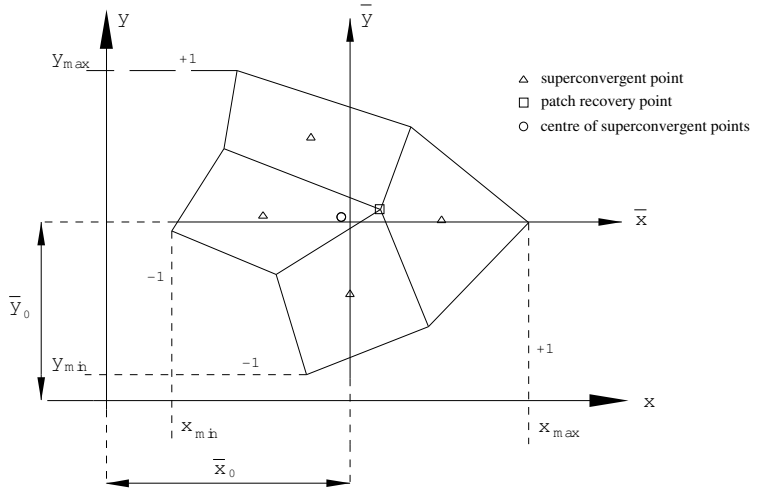

Figure 4 The normalized local patch co-ordinate system of Zienkiewicz, Zhu and Wu [5]

The equations of transformation between a co-ordinate system (x, y) and this normalized local patch co-ordinate system $(\bar{x}, \bar{y})$ are:

$$\bar{x} = -1 + 2\frac{x - x_{\min}}{x_{\max} - x_{\min}} \qquad \text{and} \qquad \bar{y} = -1 + 2\frac{y - y_{\min}}{y_{\max} - y_{\min}} \tag{8}$$

The row vector $\lfloor P \rfloor$ used in Equations (2) and (3) is now written in the co-ordinates $(\bar{x}, \bar{y})$ such that $\lfloor P \rfloor = \lfloor 1, \bar{x}, \bar{y}, \bar{x}\bar{y} \rfloor$.

c) Dependence on orientation (θ-dependence)

Although the use of a normalized local patch co-ordinate system avoids the potential problems associated with the position and size of the patch, problems associated with the orientation of the element patch (θ-dependence) with respect to this co-ordinate system can still occur. In order to demonstrate this phenomenon consider the patch of elements shown in Figure 5.

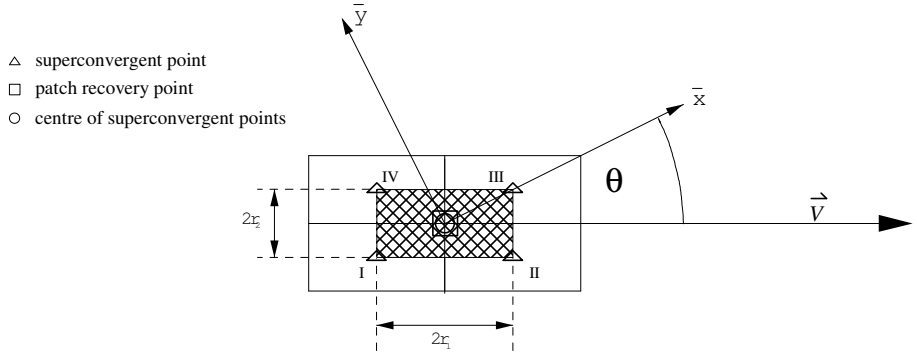

Figure 5 Element patch to show dependence on orientation of the patch

In this figure the $\bar{x}$-axis of the normalized local patch co-ordinate system $(\bar{x}, \bar{y})$ is rotated an angle θ from a vector $\dot{v}$ that is fixed in the element patch such that its origin is at the patch recovery point and is directed through the centre of a line running between the superconvergent points II and III.

For this case the matrix $[A]$, which is defined in the co-ordinate system $(\bar{x}, \bar{y})$ can be written as:

$$[A]=\begin{bmatrix} 4 & 0 & 0 & \Delta_1 \\ 0 & \Delta_2 & \Delta_1 & 0 \\ 0 & \Delta_1 & \Delta_3 & 0 \\ \Delta_1 & 0 & 0 & \Delta_4 \end{bmatrix} \tag{9}$$

where

$$\Delta_1 = -\frac{4cs(r_1 - r_2)(r_1 + r_2)}{z_1 z_2}$$

$$\Delta_2 = 4 - \frac{8csr_1 r_2}{z_1^2} \quad , \quad \Delta_3 = 4 - \frac{8csr_1 r_2}{z_2^2}$$

$$\Delta_4 = \frac{4r_1^2 r_2^2 (c^4 + s^4) + 4c^2 s^2 (r_1^4 + r_2^4 - 4r_1^2 r_2^2)}{z_1^2 z_2^2}$$

$z_1 = (cr_1 + sr_2),\ z_2 = (sr_1 + cr_2)$ and $c = \cos\theta$ and $s = \sin\theta$.

For $\theta = \frac{\pi}{4} + n\frac{\pi}{2}$, where n is an integer, $|\cos\theta| = |\sin\theta|$ and

$$\Delta_4 = \frac{4s^4 (r_1 - r_2)^2 (r_1 + r_2)^2}{z_1^2 z_2^2} = \frac{\Delta_1^2}{4} \tag{10}$$

It is observed that the components

$$A_{4,i} = \frac{\Delta_1}{4} A_{1,i} \text{ where } i = 1,2,3 \text{ or } 4 \tag{11}$$

showing that there is a linear dependence between rows 1&4. Now, although this singularity only occurs when $\theta = \frac{\pi}{4} + n\frac{\pi}{2}$ the value of the recovered stress is strongly dependent upon the angle θ. It is recorded that angles of $\theta = \frac{\pi}{4} + n\frac{\pi}{2}$ can occur in practical problems c.f. Part IV, Problem 3 and Mesh 3 of [3]. Indeed, it was this particular problem that demonstrated to the authors that the recovered stress could be dependent on the choice of co-ordinate system. This point is demonstrated with an example. Consider the rectangular patch of elements shown in Figure 5 with $r_1 = 80m$ and $r_2 = 40m$. The values of the finite element stress at the four superconvergent points are chosen arbitrarily as $\sigma_{hI} = 200MPa,\ \sigma_{hII} = 100MPa,\ \sigma_{hIII} = 500MPa$ and $\sigma_{hIV} = 150MPa$.

The condition number (defined as the ratio of the largest singular value to the smallest singular value) of the matrix $[A]$ has been plotted in Figure 6(b) and the singularity at $\theta = 45°$ is clearly visible. The singularity is localised to this angle alone but for angles that are very close to 45° the matrix $[A]$ is ill-conditioned.

The bi-linear stress surface σ_p is fitted to the superconvergent stress values and it is seen, by observing Figure 6(a), that even though the finite element stresses at the superconvergent points to which the surface is fitted are always the same, independent of the orientation, the recovered stress is strongly dependent on the angle θ even where the matrix $[A]$ is well conditioned (i.e. away from

45°). The reason for this behaviour is that the bi-linear stress surface defined in Equation (2) is not invariant to rotation. This is demonstrated graphically in Figures 6(c)-(h) which shows the stress surface σ_p for various angles between 0 and 90°. The recovered stress values are also shown.

THE PARENT PATCH CONCEPT

In order to remove the dependence of the recovered stress on the orientation of the patch co-ordinate system $(\bar{x}, \bar{y})$, the concept of the parent element [6], as used in the isoparametric mapping of four-node quadrilateral elements, is appropriated and applied to the element patch. The resulting *parent patch a*nd its associated curvilinear co-ordinate system (ξ, η) are shown in Figure 7.

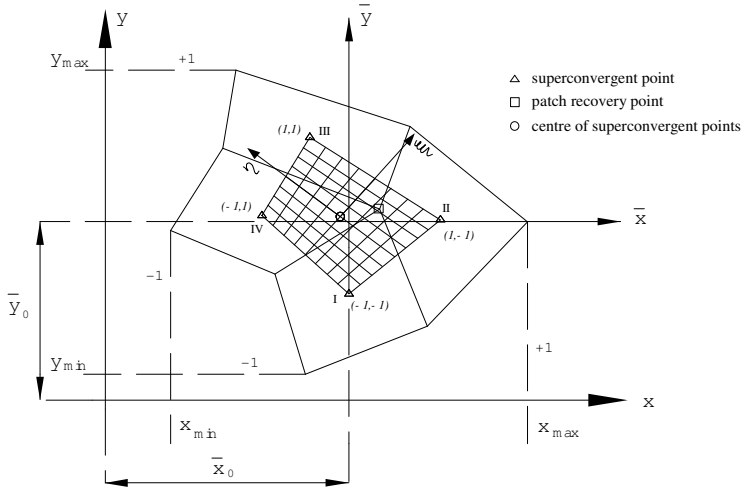

Figure 7 The parent patch and associated curvilinear co-ordinate system

The origin of the curvilinear co-ordinate system (ξ, η) is at the centre of the superconvergent points. The ξ-axis is directed through the intersection of the line running between the superconvergent points II and III and its bisector whilst the η-axis is directed through the intersection of the line running between the superconvergent points III and IV and its bisector. The equations of transformation between a co-ordinate system (x, y) and this curvilinear patch co-ordinate system (ξ, η) are:

$$\begin{aligned} x &= e_1 + e_2\xi + e_3\eta + e_4\xi\eta \\ y &= f_1 + f_2\xi + f_3\eta + f_4\xi\eta \end{aligned} \tag{12}$$

where

$$e_1 = \frac{1}{4}(+x_I + x_{II} + x_{III} + x_{IV}) \qquad f_1 = \frac{1}{4}(+y_I + y_{II} + y_{III} + y_{IV})$$

$$e_2 = \frac{1}{4}(-x_I + x_{II} + x_{III} - x_{IV}) \qquad f_2 = \frac{1}{4}(-y_I + y_{II} + y_{III} - y_{IV})$$

$$e_3 = \frac{1}{4}(-x_I - x_{II} + x_{III} + x_{IV}) \qquad f_3 = \frac{1}{4}(-y_I - y_{II} + y_{III} + y_{IV})$$

$$e_4 = \frac{1}{4}(+x_I - x_{II} + x_{III} - x_{IV}) \qquad f_4 = \frac{1}{4}(+y_I - y_{II} + y_{III} - y_{IV})$$

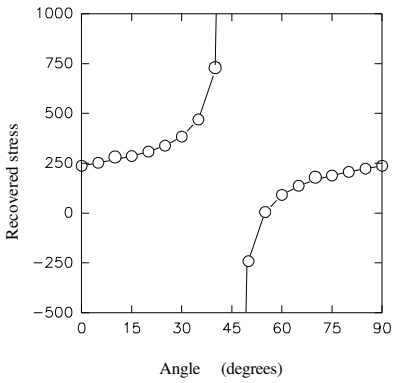

(a) Recovered stress versus θ

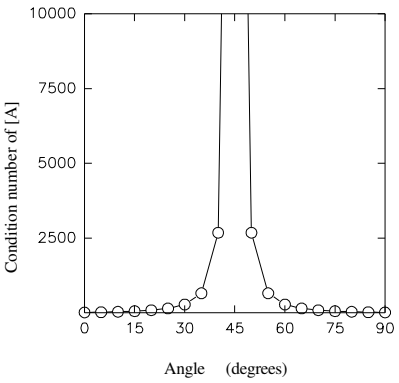

(b) Condition number versus θ

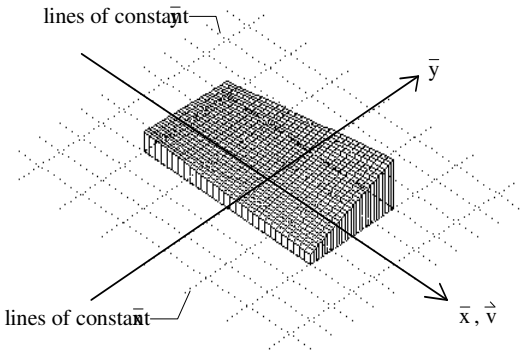

(c) $\theta = 0,\ \sigma_p = 237.5 MPa$

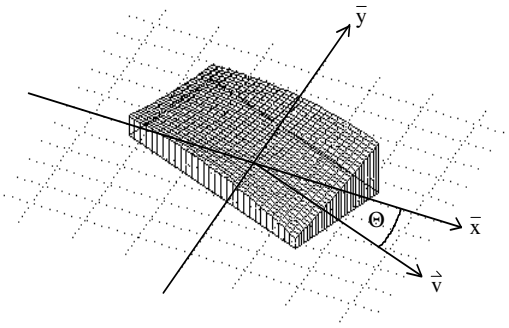

(d) $\theta = 20°,\ \sigma_p = 308.3 MPa$

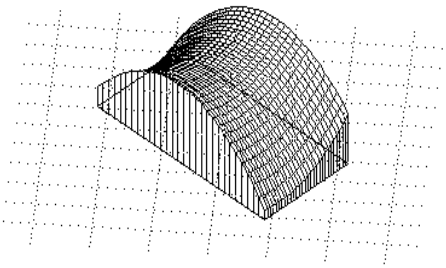

(e) $\theta = 40°,\ \sigma_p = 716.0 MPa$

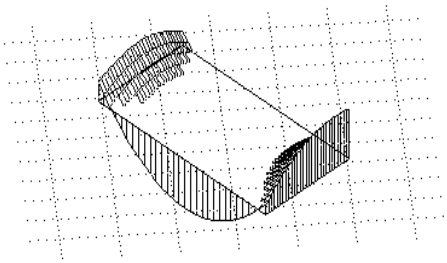

(f) $\theta = 50°,\ \sigma_p = -241.0 MPa$

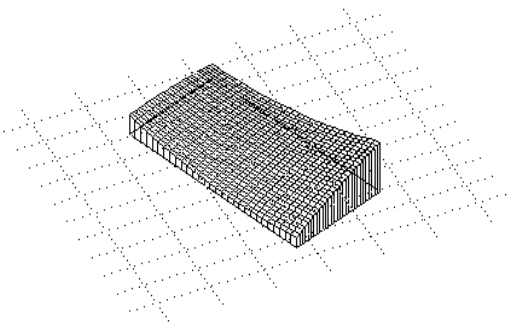

(g) $\theta = 70°,\ \sigma_p = 166.7 MPa$

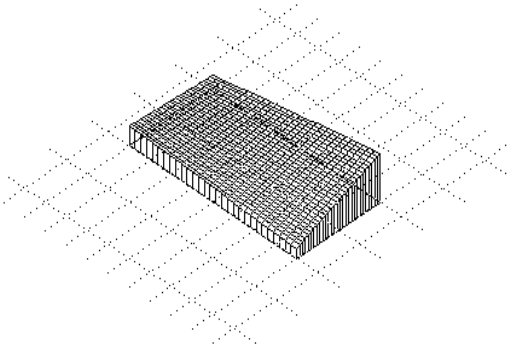

(h) $\theta = 90°,\ \sigma_p = 237.5 MPa$

Figure 6 Dependence of the stress surface on orientation of patch

In the curvilinear co-ordinate system (ξ, η) the superconvergent points then have the simple unit co-ordinates as shown in the figure.

The row vector $\lfloor P \rfloor$ is now written in terms of the co-ordinates (ξ, η) as $\lfloor P \rfloor = \lfloor 1, \xi, \eta, \xi\eta \rfloor$. The matrix $[A]$ becomes $4[I]$ where $[I]$ is the identity matrix and is independent of the real patch of elements. As such, the components of the vector $\{a\}$ may be written explicitly as:

$$
\begin{aligned}
a_1 &= \frac{1}{4}(+\sigma_{hI} + \sigma_{hII} + \sigma_{hIII} + \sigma_{hIV}) \\
a_2 &= \frac{1}{4}(-\sigma_{hI} + \sigma_{hII} + \sigma_{hIII} - \sigma_{hIV}) \\
a_3 &= \frac{1}{4}(-\sigma_{hI} - \sigma_{hII} + \sigma_{hIII} + \sigma_{hIV}) \\
a_4 &= \frac{1}{4}(+\sigma_{hI} - \sigma_{hII} + \sigma_{hIII} - \sigma_{hIV})
\end{aligned}
\tag{13}
$$

It is observed that the value of the stress surface σ_p at the centre of the superconvergent points $(\xi = \eta = 0)$ is simply the average of the values at the four superconvergent points. Thus, for four elements having superconvergent points forming a parallelogram, the superconvergent point is coincident with the patch recovery point and the recovered stress is simply the average of the values of the finite element stress at the four superconvergent points. For an arbitrary distribution of superconvergent points, the centre of the superconvergent points is no longer coincident with the patch recovery point and the recovered stress is determined by evaluating Equation (2) at the stress recovery point after first solving Equation (12) for the curvilinear co-ordinates of the patch recovery point. This requires the solution of a pair of non-linear equations and can be done using a simple iterative technique such as Newton-Raphson [7].

With the parent patch concept the matrix $[A]$ is never singular or ill-conditioned and there is always a unique value for the recovered stress.

Thus far we have only considered the patch recovery scheme as it applies to internal nodes. The recovered stress for internal nodes is obtained by *interpolating* from the stress surface σ_p. For boundary nodes the recovered stress is obtained by *extrapolating* from the appropriate stress surface. For corner nodes, i.e. those nodes belonging to a single element, the appropriate stress surface is the one defined using the superconvergent point for that element. For other boundary nodes belonging to two elements the appropriate stress surface is the one that is defined using the superconvergent points of both elements.

In Part II of this article the results for an error estimator based on the patch recovery scheme and using the concept of the parent patch will be presented and discussed.

****

SOME STUDIES OF AN ERROR ESTIMATOR BASED ON A PATCH RECOVERY SCHEME
PART II - AN ERROR ESTIMATOR BASED ON THE PATCH RECOVERY SCHEME

by A.C.A. Ramsay & H. Sbresny

****

THE ERROR ESTIMATOR

An error estimator Ep based on the patch recovery scheme of [4] but using the concept of the parent patch is defined. This error estimator will be tested on three plane elasticity problems:

1) Rectangular continuum convergence problem
2) Rectangular continuum distortion problem
3) Stress concentration problem

In addition, the results for another error estimator E3 will also be presented. This error estimator was discussed in detail in [3]. Both error estimators Ep and E3 use estimated stress fields that are continuous in the sense of Equation (1). For Ep the unique nodal stresses $\{s\}$ are determined from the patch recovery scheme using the concept of the parent patch whilst for E3, $\{s\}$ is taken as the nodal average of the finite element stresses evaluated directly at the nodes (SRS1 [3]).

In evaluating and comparing the error estimators use shall be made of the error measures and effectivity ratio defined in [3]. For completeness these are now summarised.

The true percentage error α for a group of elements is defined as

$$\alpha = \frac{U_e}{U} \times 100\% \tag{14}$$

where U is the true strain energy. The strain energy of the true error is $U_e = U - U_h$ where U_h is the finite element strain energy and is integrated using 5x5 Gauss quadrature for reasons explained in [3].

The estimated percentage error $\tilde{\alpha}$ for the group of elements is defined as

$$\tilde{\alpha} = \frac{\tilde{U}_e}{U_h + \tilde{U}_e} \times 100\% \tag{15}$$

where the strain energy of the estimated error is $\tilde{U}_e = \frac{1}{2}\int_V \{\tilde{\sigma}_e\}^T \{\tilde{\varepsilon}_e\} dV$ (V is the volume of the group of elements) and is integrated using 2x2 Gauss quadrature. For $\tilde{\alpha}$ the finite element strain energy is integrated using 2x2 Gauss quadrature ([3]).

The effectivity of an error estimator is measured with the effectivity ratio which is defined as

$$\beta = \frac{\tilde{U}_e}{U_e} \tag{16}$$

Error measures and effectivity ratios corresponding to error estimators Ep and E3 will be denoted with a subscript Ep and E3 respectively. In addition to the integrated error measures α and $\tilde{\alpha}$, we shall also investigate the pointwise quality of the estimated stress field. It has been claimed in [4] that because the unique nodal stresses from the patch recovery scheme have either been extrapolated

(for boundary nodes) or interpolated (for internal nodes) from a stress surface that has been fitted to finite element stresses that are superconvergent then so the recovered stresses should also possess the superconvergent quality. The rates of convergence of pointwise stress will be examined for the two error estimators studied in this article. In examining the rate of convergence of the estimated stress at a point, the *error in the estimated stress* $\{\hat{\sigma}\}$ will be required and is defined as

$$\{\hat{\sigma}\} = \{\sigma\} - \{\tilde{\sigma}\} = \{\sigma_e\} - \{\tilde{\sigma}_e\} \tag{17}$$

Where stress fields and components of stress at a point are discussed, the superscripts Ep and E3 will denote the particular error estimator used.

PROBLEM 1: RECTANGULAR CONTINUUM CONVERGENCE PROBLEM

To demonstrate how the error measures converge as a finite element mesh is refined, a rectangular continuum problem is investigated as shown in Figure 8(a). Plane stress is assumed with Young's Modulus $E = 210\,N/m^2$, Poisson's Ratio $\nu = 0.3$ and material thickness $t = 0.1m$. The applied static boundary conditions and the known analytical solution are given in the figure.

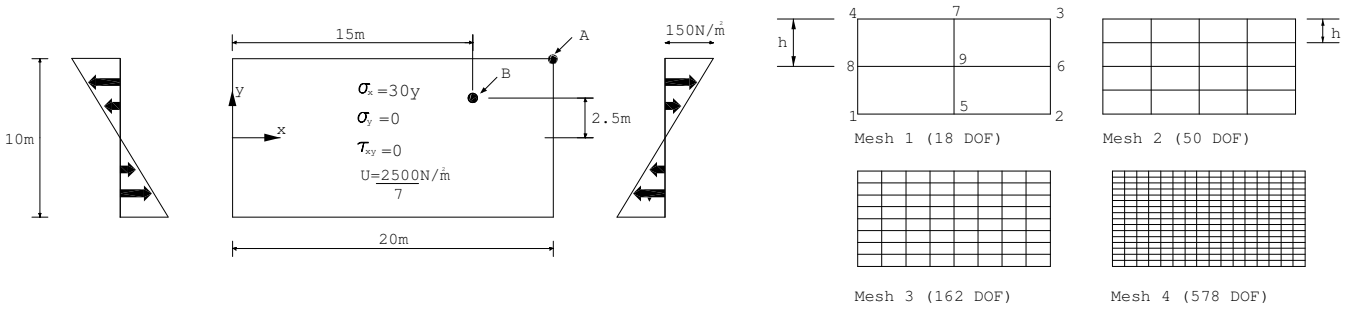

(a) The problem (b) The meshes

Figure 8 Rectangular continuum convergence problem

Four levels of mesh refinement are considered. Since neither error estimator is able to detect error for a single element the initial mesh (Mesh 1) consists of 2x2 rectangular elements. The remaining three meshes are achieved through uniform refinement of Mesh 1 and are shown in Figure 8(b).

The error measures, effectivity ratios, and the *x*-component of the error in the estimated stress $\hat{\sigma}_x$ at points A and B are shown in Table 1. The column headed h lists the characteristic length of a typical element in the mesh and for this problem is taken as the y-dimension of an element (all elements being identical in size). The dimension h is illustrated for Mesh 1 & 2 in Figure 8(b).

Table 1 Results for rectangular continuum problem

			Error measures			Effectivity ratios		Point A		Point B	
Mesh	DOF	h	α	$\tilde{\alpha}_{E3}$	$\tilde{\alpha}_{Ep}$	β_{E3}	β_{Ep}	$\hat{\sigma}_x^{E3}$	$\hat{\sigma}_x^{Ep}$	$\hat{\sigma}_x^{E3}$	$\hat{\sigma}_x^{Ep}$
1(2x2)	18	5	29.05	22.51	22.51	0.71	0.71	38.3	43.57	\	\
2(4x4)	50	2.5	9.16	8.38	8.42	0.91	0.91	14.4	15.61	5.38	6.53
3(8x8)	162	1.25	2.47	2.41	2.41	0.97	0.97	6.08	7.71	1.52	1.70
4(16x16)	578	0.625	0.63	0.63	0.63	0.99	0.99	2.95	3.91	0.34	0.44

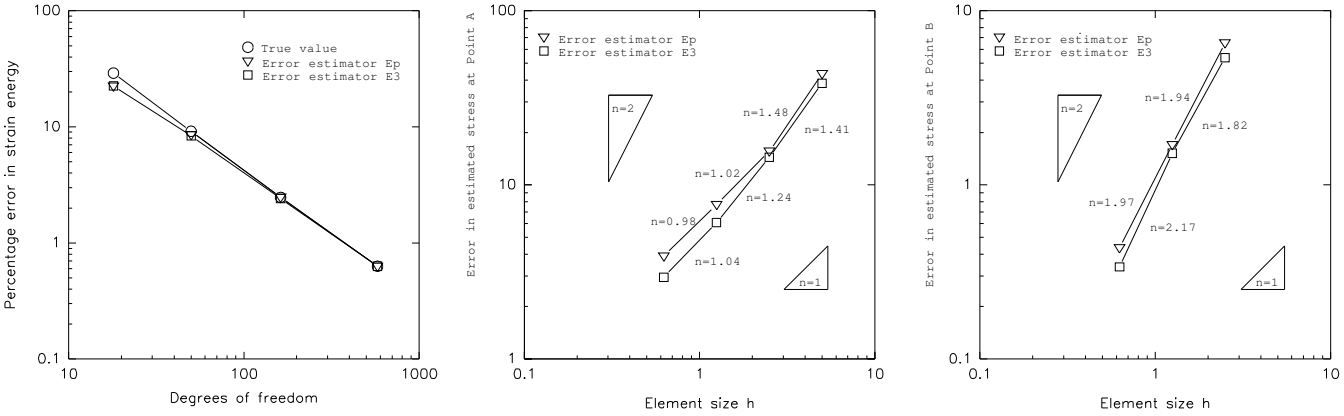

(a) Error measures (b) $\hat{\sigma}_x$ at Point A (c) $\hat{\sigma}_x$ at Point B

Figure 9 Convergence characteristics for rectangular continuum problem

Considering the results shown in Table 1 and Figure 9 the following observations are made:

(i) For Mesh 1 error measures $\tilde{\alpha}_{E3}$ and $\tilde{\alpha}_{Ep}$ are equal (at least to the 2 decimal places reported here). This means that the strain energy of the estimated error $\tilde{U}_e$ is also equal for the two error estimators. Such an observation might lead one to reason that the estimated stress fields $\{\tilde{\sigma}\}^{E3}$ and $\{\tilde{\sigma}\}^{Ep}$ are also identical in a pointwise sense. However this is not the case as can be seen by observing the unique nodal stresses as given in Table 2.

Table 2 Unique nodal stresses for Mesh 1

	Error estimator E3			Error estimator Ep		
Node	$\tilde{\sigma}_x$	$\tilde{\sigma}_y$	$\tilde{\tau}_{xy}$	$\tilde{\sigma}_x$	$\tilde{\sigma}_y$	$\tilde{\tau}_{xy}$
1	-111.7	-17.5	-40.9	-106.4	0	0
2	-111.7	-17.5	40.9	-106.4	0	0
3	111.7	17.5	40.9	106.4	0	0
4	111.7	17.5	-40.9	106.4	0	0
5	-111.7	-17.5	0	-106.4	0	0
6	0	0	40.9	0	0	0
7	111.7	17.5	0	106.4	0	0
8	0	0	-40.9	0	0	0
9	0	0	0	0	0	0

This situation provides an example of the way in which, when integrated, two different stress fields can yield the same value.

(ii) Consider now the pointwise quality of the estimated stress fields. Table 1 shows the x-component of the error in the estimated stress $\hat{\sigma}_x$ at points A and B (see Figure 8(a)). Figure 9(b) shows the way in which $\hat{\sigma}_x$ varies with h for Point A. There is no patch recovery point at Point B for Mesh 1 and the variation of $\$_x$ with h for meshes 2,3 & 4 is shown in Figure 9(c). Figures 9(b)

& (c) are plotted using logarithmic scales such that the gradient of the graph then represents the rate of convergence of $\hat{\sigma}_x$.

The rate of convergence varies for different meshes but tends to a constant value, called the *theoretical rate of convergence*, as the mesh is refined ($h \to 0$). For the element considered in this article the theoretical rate of convergence for a pointwise component of stress is $n = 1$. For the superconvergent points the rate of convergence is one order higher than theoretical ie $n = 2$. For the element under consideration there is a single superconvergent point at the isoparametric centre of the element. The gradients corresponding to the theoretical and superconvergent rates of convergence are illustrated with triangular wedges in Figures 9(b) & (c).

For Point B it is seen that the error in estimated stress $\hat{\sigma}_x$ for both error estimators appears to be reaching the superconvergent rate of convergence of *n*=2 as the mesh is refined with error estimator E3 giving the slightly superior results. For Point A, it is observed that the error in estimated stress $\hat{\sigma}_x$ for both error estimators appears to be reaching the theoretical rate of convergence of *n*=1 as the mesh is refined. Again error estimator E3 gives slightly superior results.

(iii) The effectivity ratios of both error estimators appear to be converging to unity as the mesh is refined. Error estimators exhibiting such behaviour are termed asymptotically exact error estimators.

PROBLEM 2: RECTANGULAR CONTINUUM DISTORTION PROBLEM

The performance of the error estimators for a distorted mesh is now examined. The rectangular continuum convergence problem with Mesh 1 is considered but now the mesh is distorted as shown in Figure 10. Five levels of distortion will be considered with *d* varying between 0 and 4*m* in unit increments.

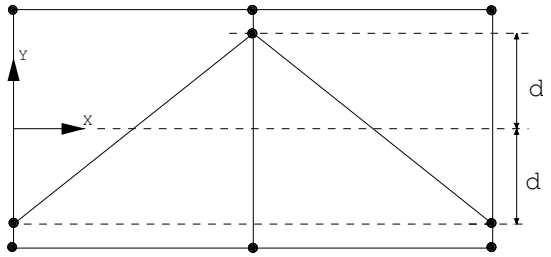

Figure 10 Mesh configuration for distortion tests

Table 3 Results for distortion problem

	Error measures			Effectivity ratios	
d	α	$\tilde{\alpha}_{E3}$	$\tilde{\alpha}_{Ep}$	β_{E3}	β_{Ep}
0	29.04	22.51	22.51	0.71	0.71
1	30.91	21.89	24.62	0.63	0.72
2	36.49	20.82	30.42	0.45	0.74
3	45.53	21.48	38.34	0.32	0.71
4	57.05	29.04	46.27	0.30	0.62

The results for this problem are shown in Table 3 and have been plotted in Figure 11. It was observed in [3] that the decreasing effectivity of the error estimator E3 with distortion was due to the fact that as the mesh was distorted the finite element stress field, whilst moving further away from the true solution, also became smoother. In contrast to this, error estimator Ep appears able to maintain a fairly constant level of effectivity (cf. Figure 13(b)) independent of distortion. The reason for this can be found by comparing the estimated error stress field with the true error stress field as is shown in Figure 12.

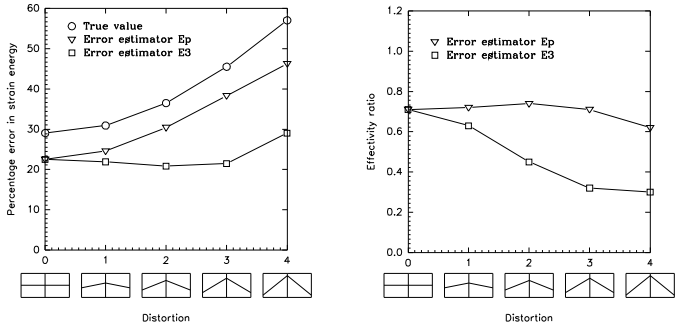

(a) Error measures (b) Effectivity ratios

Figure 11 Error measures and effectivity ratios for distortion problem

PROBLEM 3: STRESS CONCENTRATION PROBLEM

In this problem the performance of the error estimators for a problem involving a stress concentration is examined. The problem studied is the classical problem of a square plate with a central circular hole subjected to uniform tensile boundary tractions as shown in Figure 13(a). Plane stress is assumed with Young's Modulus $E = 10\,MN/m^2$, Poisson's Ratio $\nu = 0.25$ and a material thickness of $t = 0.01m$. There is no analytical solution to this problem when the dimensions of the plate are finite. However, lower and upper bounds to the true strain energy have been obtained by using compatible and equilibrium finite element models respectively on the refined mesh shown in the first quadrant of Figure 13(a). For the equilibrium model the piecewise linear membrane element of Maunder [8] has been used. The true strain energy (for the quarter model) is thus bounded as $5.5245 \le U \le 5.5294\ \ Nm$. Due to the symmetry of this problem only one quarter of the domain need be modelled. Four meshes are considered as shown in Figure 13(b).

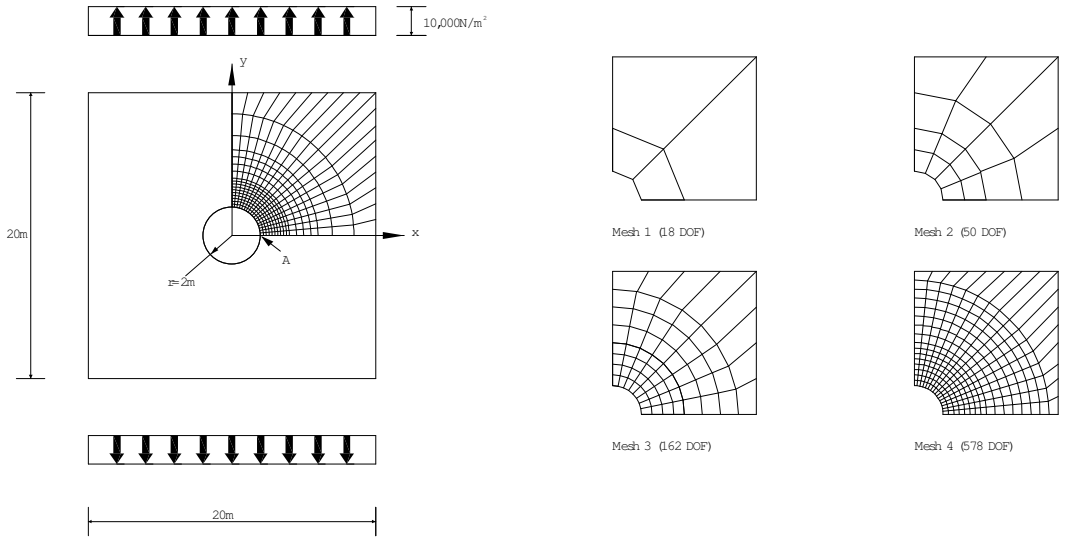

(a) The problem (b) The meshes

Figure 13 Stress concentration problem

The results for this problem are shown in Table 4 and Figure 14. Two values are tabulated for the percentage error α and the effectivity ratios β_{E3} and β_{Ep}. These values correspond to the upper and lower bounds on the true strain energy with the values in parentheses being those corresponding to the lower bound on *U*.

Table 4 Results for stress concentration problem

		Error measures			Effectivity ratios		Point A	
Mesh	DOF	α	$\tilde{\alpha}_{E3}$	$\tilde{\alpha}_{Ep}$	β_{E3}	β_{Ep}	$\tilde{\sigma}_y^{E3}$	$\tilde{\sigma}_y^{Ep}$
1	18	3.205 (3.121)	0.790	4.457	0.240 (0.247)	1.393 (1.431)	24,834	19,654
2	50	1.354 (1.268)	0.612	0.916	0.449 (0.479)	0.669 (0.713)	29,689	25,312
3	162	0.441 (0.354)	0.271	0.343	0.616 (0.767)	0.774 (0.963)	32,895	29,349
4	578	0.121 (0.034)	0.091	0.104	0.755 (2.672)	0.852 (2.975)	33,917	31,808

In Figure 14(c) the *y*-component of the estimated stress at Point A is plotted against degrees of freedom. Since the true stress at this point is not known the rate of convergence cannot be determined.

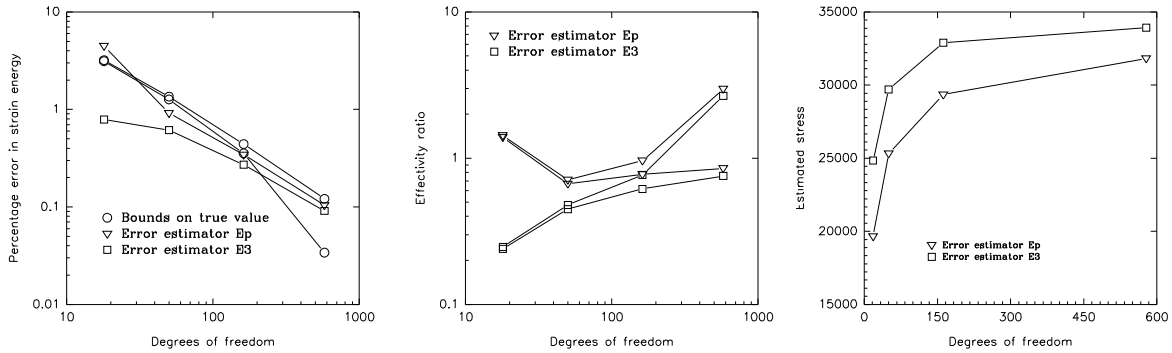

(a) Percentage error (b) Effectivity ratios (c) Estimated stress

Figure 14 Convergence of results for stress concentration problem

Observing the results for the stress concentration problem leads to the following observations:

(i) neither error estimator appears to be asymptotically exact

(ii) The estimated stress field for Ep at points of stress concentration appears to be fairly poor

CONCLUSIONS

This article has demonstrated how, for the four-node isoparametric displacement membrane and for a configuration of four elements, the patch recovery scheme as proposed in [4] can produce results that are dependent on the orientation of the patch in the recommended normalized local patch co-ordinate system of [5]. In order to overcome this problem the concept of the parent patch was introduced and it was found that this method produced results that were invariant to the orientation of the co-ordinate system.

An error estimator Ep using the concept of the parent patch was defined and tested on three plane elasticity problems and compared with another error estimator E3. Through these tests the following conclusions can be drawn:

(i) Although for some problems (cf. Problem 1) the error estimator Ep did appear to be asymptotically exact, for others (cf. Problem 3) it did not.

(ii) For problems in which the elements are severely distorted (cf. Problem 2) it was seen that the error estimator Ep performed better then E3.

(iii) The claim made in [4] that the recovered stresses are generally superconvergent has been demonstrated to be false for the patch recovery scheme using the parent patch concept. Indeed, for the two convergence problems investigated (Problems 1 & 3) it was observed that the recovered stresses of error estimator Ep were inferior to those of E3 that are recovered by simple nodal averaging of the finite element stresses evaluated directly at the nodes.

(iv) It was observed that for parallelogram elements, the recovered stress obtained using the parent patch concept was simply the average of the superconvergent stress values in the patch of elements. This has some important implications. The parent patch concept may only be suitable for the type and configuration of elements discussed in this article. However, for other elements and configurations it might prove fruitful to examine patch recovery schemes that simply take the average of the 'ring' of superconvergent points that surround the patch recovery point. For example consider the case of the eight-node displacement membrane.

ACKNOWLEDGEMENTS

The authors would like to acknowledge Professor J. Robinson of the Robinson FEM Institute and Dr E.A.W. Maunder of the University of Exeter for their help and encouragement offered in preparing this article. The first author wishes it to be recorded that financial support for this work has been provided jointly by the SERC and Nuclear Electric plc. To these organisations he is grateful.

REFERENCES

[1] O.C. Zienkiewicz and J.Z. Zhu, 'A Simple Error Estimator and Adaptive Procedure for Practical Engineering Analysis', Int. J. Num. Meth. Eng., **24**, 337-357 (1987)

[2] E. Hinton and J.S. Campbell, 'Local and Global Smoothing of Discontinuous Finite Element Functions using a Least Square Method', Int. J. Num. Meth. Eng., **8**, 461-480 (1974)

[3] J. Robinson, E.A.W. Maunder, A.C.A. Ramsay, 'Some Studies of Simple Error Estimators', Parts I-VI, Finite Element News, 1992-1993, Issues No.4-2

[4] O.C. Zienkiewicz and J.Z. Zhu, 'The Superconvergent Patch Recovery and *a posteriori* Error Estimates. Part I: The Recovery Technique', Int. J. Num. Meth. Eng., **33**, 1331-1364 (1992)

[5] O.C. Zienkiewicz, J.Z. Zhu and J. Wu, 'Superconvergent Patch Recovery Techniques-Some Further Tests', Comm. Num. Meth. Eng., **9**, 251-258 (1993)

[6] D.S. Burnett, 'Finite Element Analysis', Addison-Wesley, (1987)

[7] S.C. Chapra and R.P. Canale, 'Numerical Methods for Engineers', McGraw-Hill, (1988)